Proceedings of the ASME 28th International Conference on Ocean, Offshore and Arctic Engineering
OMAE2009
May 31 - June 5, 2009, Honolulu, Hawaii, USA

OMAE2009-79051

NUMERICAL SIMULATION OF SLOSHING IN A TANK, CFD CALCULATIONS AGAINST MODEL TESTS

Bogdan Iwanowski*
FORCE Technology Norway AS
Claude Monets alle 5
1338 Sandvika
Norway
Email: boi@force.no

Marc Lefranc
FORCE Technology Norway AS
Email: mrl@force.no

Rik Wemmenhove
FORCE Technology Norway AS
Email: riw@force.no

ABSTRACT

Simulation of liquid dynamics in an LNG tank is studied numerically. The applied CFD code solves Navier-Stokes equations and uses an improved Volume of Fluid (iVOF) method to track movement of fluid's free surface. Relative advantages of using two different fluid models, single-phase (liquid+void) and two-phase (liquid+compressible gas) are discussed, the latter model being capable of simulating bubbles and gas entrapped in liquid. Furthermore, the 1st and 2nd order upwind differencing schemes are used with both physical models leading to a total of four possible approaches to solve the problem.

Numerical results are verified against experimental data from large scale (1:10) sloshing experiments of 2D section of an LNG carrier. The CFD vs. experiment comparison is shown for tank filling rates of practical interest, ranging from 10% to 95%, and includes both fluid height and fluid pressure exerted on tank walls. A visual comparison in form of computer animation frames, synchronised with camera-made movies taken during the experiments is included as well. Finally, an exhaustive computational grid convergence study is presented for lower filling rates of the tank.

INTRODUCTION

Sloshing of liquids in an oscillating tank is one of important engineering problems encountered in marine industry. Typical examples of marine structures that can be affected by sloshing are LNG carriers and FPSO units. A violent sloshing motion can produce excessively high fluid impact pressures on the tank's walls or break internal pipelines.

A number of numerical methods having the goal of computing violent fluid motion in a moving tank have been proposed in recent years, [1–4], only to quote a few. One of such methods is the ComFLOW code, which solves Navier-Stokes equations and applies an improved Volume of Fluid (iVOF) method to follow movement of fluid's free surface.

A numerical method should be validated. Main purpose of this paper is presentation of ComFLOW numerical simulatons' results confronted with data obtained from large scale (1:10) sloshing experiments of 2D section of a typical LNG carrier.

THE COMFLOW PROGRAM

The 3D CFD solver ComFLOW has been developed by University of Groningen, The Netherlands. It introduces a local height function as an improvement over the original VOF algorithm [5]. The code has been continuously and actively developed within Joint Industry Projects SAFE-FLOW (2001-2004) and ComFLOW-2 (2005-2008).

MATHEMATICAL MODELS

The ComFLOW program can employ one of two basic physical models, either single-phase (liquid+void) or two-phase fluid

*Address all correspondence to this author.

flow (liquid+compressible gas). The latter model seems to be necessary for sloshing calculations with higher fluid filling rates. It is understood that "liquid" is an incompressible heavy fluid, such as water or liquefied natural gas (LNG). The compressible gas phase can be either air or an LNG vapour. Basic equations for both models are discussed briefly since results from both approaches will be presented in the paper.

Single-Phase Flow

Flow of an incompressible fluid, in an arbitrary three-dimensional domain can be found by solving continuity equation, Eqn. (1), together with Navier-Stokes equations describing conservation of momentum, Eqn. (2):

$$\nabla \cdot \mathbf{u} \;=\; 0 \tag{1}$$

where $\mathbf{u} = (u, v, w)$ is fluid's velocity vector.

$$\frac{\partial \mathbf{u}}{\partial t} \;+\; \mathbf{u} \cdot \nabla \mathbf{u} \;=\; -\frac{1}{\rho} \nabla p \;+\; \frac{\mu}{\rho} \nabla \cdot \nabla \mathbf{u} \;+\; \mathbf{G} \tag{2}$$

with p being fluid's pressure, ρ its constant density and μ its constant dynamic viscosity coefficient. Further, t is time and $\mathbf{G} = (G_x, G_y, G_z)$ is an external body force, for example gravity. Further details of the single-phase algorithms used in ComFLOW can be found in [6, 7].

Two-Phase Flow

The two-phase flow is distinct due to one crucial change, namely, the gas phase is compressible. The continuity equation and Navier-Stokes equations are now Eqs. (3,4):

$$\frac{\partial \rho}{\partial t} \;+\; \nabla \cdot (\rho\, \mathbf{u}) \;=\; 0 \tag{3}$$

$$\frac{\partial (\rho \mathbf{u})}{\partial t} \;+\; \nabla \cdot (\rho \mathbf{u}\mathbf{u}) \;=\; -\nabla p + \nabla \cdot (\mu \nabla \mathbf{u}) + \rho \mathbf{G} \tag{4}$$

where meaning of all symbols is the same as for the single-phase flow model, but fluid's density ρ (and possibly dynamic coefficient of viscosity μ) are no longer constant.

For two-phase flows it is necessary to close system of equations by relating fluid's pressure and density. This relation is applied only for the compressible phase and an adiabatic equation of state is used, Eqn. (5):

$$\frac{p_{gas}}{p_{ref}} \;=\; \left(\frac{\rho_{gas}}{\rho_{ref}}\right)^{\gamma} \tag{5}$$

The two-phase algorithms used in ComFLOW are described at length in [4, 8].

Second Order Upwind Differencing

It is very well known that convective terms in Navier-Stokes equations require special attention. The often used 1^{st} order upwind differencing scheme, hereafter denoted as **B2**, introduces a large amount of artificial dissipation. Therefore, the 2^{nd} order upwind differencing scheme (denoted as **B3**) has been implemented in order to limit amount of numerical damping caused by the upwind differencing itself.

The 2^{nd} order scheme gives less numerical damping, but also requires a change in time integration algorithm. The forward Euler method involving two time levels of variables is sufficient to obtain a stable solution when **B2** is used. However, three time levels of variables and Adams-Bashforth time integration scheme are necessary for stability with **B3**. It is also noted that calculations with the **B3** scheme call for much smaller computational time step and are typically 3 $\times$ slower, and can be even 10 $\times$ slower than with the 1^{st} order scheme **B2**. The already quoted references [4, 8] can be consulted for more details.

Both time integration schemes must also satisfy the usual CFL-number and diffusive-number stability criteria.

Operational Modes of the ComFLOW Program

One can distinguish 4 possible operational modes for the ComFLOW program:

(a) 1-phase mode, liquid+void, **B2** upwind differencing scheme,
(b) 1-phase mode, liquid+void, **B3** upwind differencing scheme,
(c) 2-phase mode, liquid+compressible gas, **B2** scheme,
(d) 2-phase mode, liquid+compressible gas, **B3** scheme.

THE SLOSHING EXPERIMENTS

The large scale (1:10) sloshing experiments were performed by MARIN of The Netherlands at DnV facility in Høvik near Oslo, Norway. Main objective of these experiments was to provide validation material for the ComFLOW code and the experiments themselves were part of the ComFLOW-2 JIP. The prismatic tank was a 2D slice of a typical LNG carrier. The sloshing experiments used water and air at atmospheric pressure. A photograph of the experimental tank is shown in Fig. 1 and its main dimensions are displayed in Fig. 2. Detailed description of the experiments can be found in [9, 10] and only some facts relevant to this paper are briefly outlined.

The experimental program was quite extensive, including sway and roll motions (separate and combined) of the tank, with regular and irregular excitations. The regular sway motions of the tank have been chosen for presentation in this paper, as listed

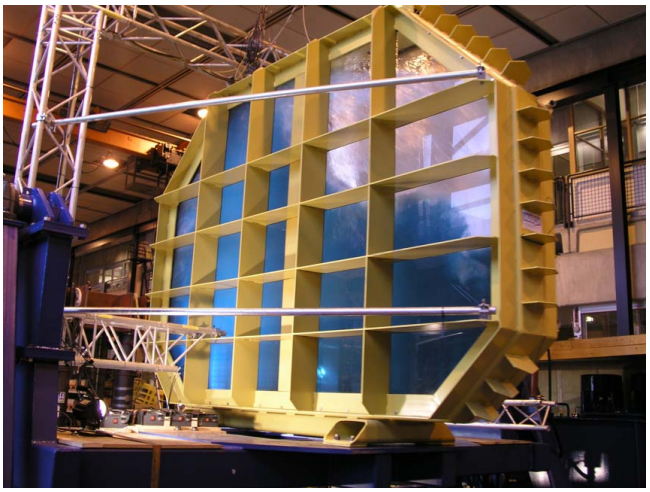

Figure 1. Experimental sloshing tank prepared by MARIN

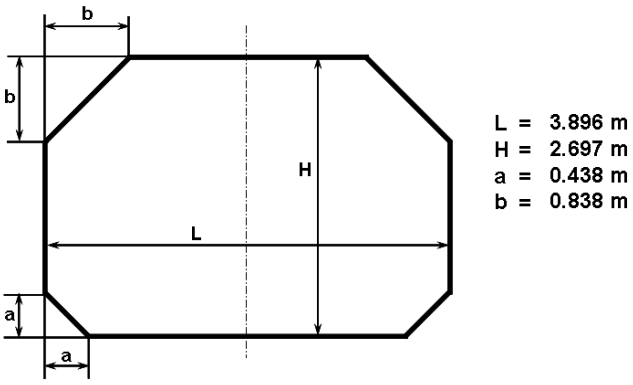

Figure 2. Experimental sloshing tank, main dimansions

in Tab. 1, where fill levels and periods of oscillation are given in model scale.

Table 1. Experiments chosen for discussion in the paper

Filling rate	Fluid fill level, [m]	Oscillation period, [sec]
10%	0.446	3.48
25%	0.674	3.13
70%	1.888	2.78
95%	2.562	2.62

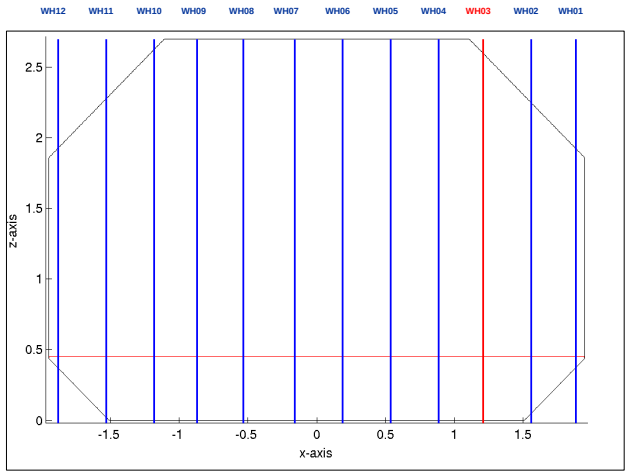

Figure 3. Locations of water height probes, all filling rates

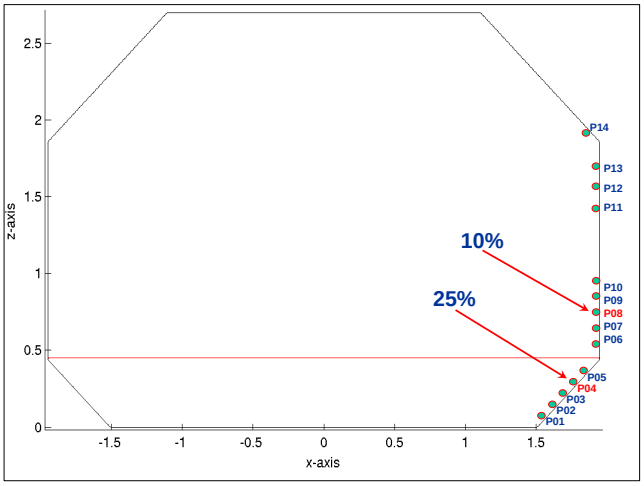

Figure 4. Pressure sensors, low filling rates 10% and 25%

Instrumentation for the Sloshing Experiments

From each experimental run, the recorded time-value traces included data about the tank motion itself, water height at 12 fluid height probes and fluid pressure at 14 pressure sensors. Locations of the water height probes were the same for each experiment and are shown in Fig. 3. Positions of the fluid pressure sensors for low filling rates of 10% and 25% are shown in Fig. 4, and for high filling rates of 70% and 95% in Fig. 5.

Hereafter, the experimental and computational results will be reported for fluid height probe WH03 (all filling rates) and for pressure sensors listed in Tab. 2. These control locations are also clearly marked in relevant Figures.

Sloshing pressures at sensor locations chosen for the 10%, 70% and 95% filling rates are mostly of dynamical kind. In contrast, the P04 sensor chosen for the 25% filling rate is submerged

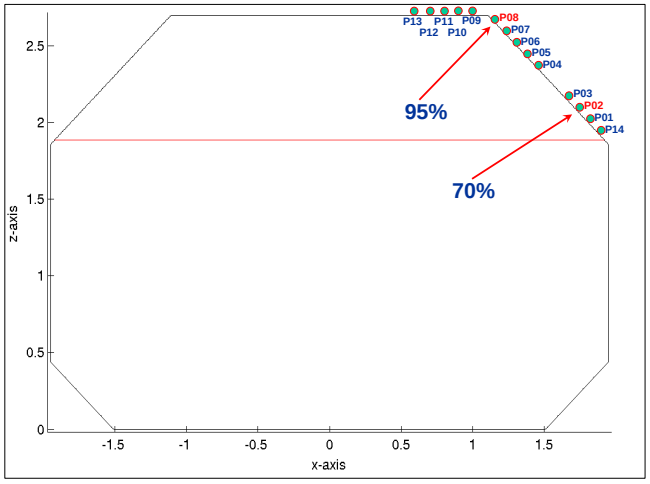

Figure 5. Pressure sensors, high filling rates 70% and 95%

and pressure there contains a hydrostatic contribution.

Table 2. Control locations where results are reported

Filling rate	Water height probe	Pressure sensor
10%	**WH03**	**P08**
25%	**WH03**	**P04**
70%	**WH03**	**P02**
95%	**WH03**	**P08**

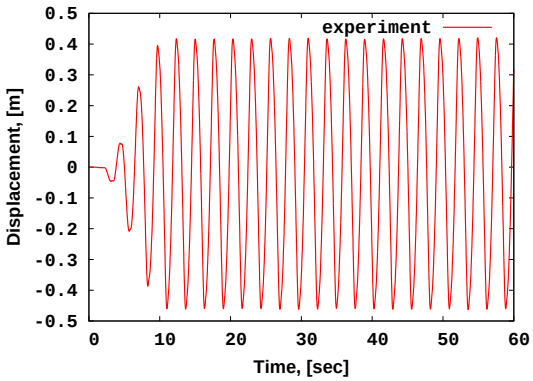

Figure 6. Tank displacement, signal obtained experimentally

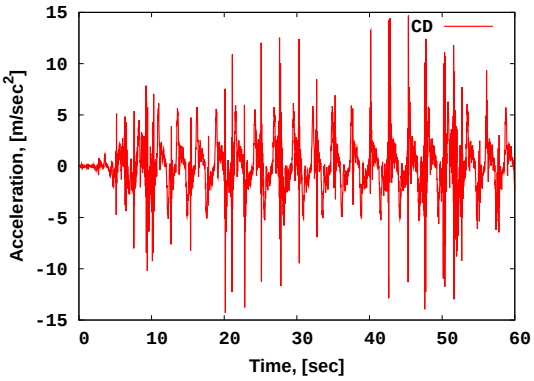

Figure 7. Tank acceleration, derived with central differences

KINEMATICS OF TANK MOTION

Motion of the tank itself, as modelled for numerical simulation of sloshing in ComFLOW, should be the same as recorded during the experiment. Although experimental data of the tank motion is available, it includes time traces of tank's displacement only. But description of moving coordinate system in ComFLOW requires time traces of tank's velocity and acceleration as well.

The experimental time traces of the tank's displacement look quite regular. An example of initial 60 seconds of the tank's motion (about 20 periods), from the 70% filling rate experiment, is shown in Fig. 6. It has been decided that the original tank's displacement signal given from the experiment should not be touched (no filtering or smoothing techniques should be applied). One can use a simple numerical differentiation with central difference formula to find tank motion velocity and acceleration (the "plain" central difference formula is hereafter referenced as CD). The acceleration obtained with such plain numerical differencing is displayed in Fig. 7 and it can be seen that the curve is quite shaky and contains numerically induced peaks. Such peaks are also visible in the (not shown) time-velocity graph, although the peaks are less severe.

Such problems are not new and there exists a bibliography concerning the subject. Two approaches have been tried in order to find a better algorithm of computing tank velocity and acceleration.

Methodology presented in [11] allows to derive a family of multi-point finite difference formulae, Eqn. (6), where h is an abscissa value increment (time step). These are generalizations of finite differences, and a "plain" central finite difference formula is recovered for n=1. Equation (6) shows calculations of the first derivative (velocity) from an array of discrete tank displacement values y_i, $i = 1,\ldots,M$. The same formula can be applied again to obtain the second derivative (acceleration).

Rational approximation, Eqn. (7), uses the original discrete

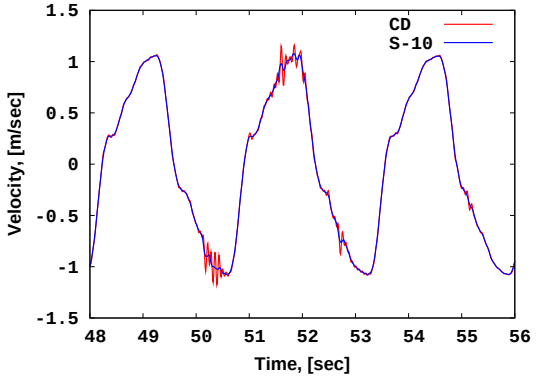

Figure 8. Tank velocity, CD and improved method S-10

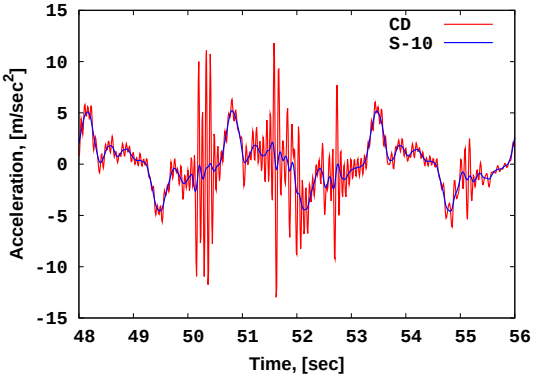

Figure 9. Tank acceleration, CD and improved method S-10

data set y_i, $i = 1,\ldots,M$ to find coefficients $a_0, a_1, a_2, \ldots$ and $b_0, b_1, b_2, \ldots$, respectively, where number of coefficients appearing in numerator/denominator should be decided in advance. The rational Chebyshev approximation iterative procedure (*Remez exchange algorithms*, [12, 13]) gives the best fit for the coefficients. A local approximation to the tank's time-displacement function is obtained and the rational polynomial can be analytically differentiated once to find velocity or twice to get acceleration.

$$\dot{y}_i(x) = \frac{\sum_{k=-n}^{k=n} k\, y_{i+k}(x)}{2\,h \sum_{k=1}^{k=n} k^2} \tag{6}$$

$$R(x) = \frac{a_0 + a_1 x + a_2 x^2 + \ldots}{b_0 + b_1 x + b_2 x^2 + \ldots} = \frac{P(x)}{Q(x)} \tag{7}$$

Numerical tests revealed that the generalized finite differences, Eqn. (6), are better suited for the problem at hand. The rational approximation approach could prove advantageous if the underlying displacement time series are un-evenly sampled, which is not the case here. Further tests have shown that Eqn. (6) with n=5 performs in a very satisfactory way (differentiation stencil width of 10, denoted hereafter as S-10).

The improved quality of the tank's velocity and acceleration calculations can be judged from Fig. (8) and Fig. (9).

SETUP OF COMPUTATIONAL GRID

The ComFLOW calculations for the fluid sloshing in a tank problem were performed to verify this code against experimental data. A systematic grid convergence approach has been adopted in order to accomplish the task. All calculations were two-dimensional, as this was idea behind the experiment.

Four computational grids have been designed for the ComFLOW sloshing calculations. The grids are described in Tab. 3. All grids are uniform, with the same grid spacing in both computational directions. It is noted that the last two grid densities are often prohibitive computationally.

Table 3. ComFLOW computational grids used in sloshing calculations

Cell size $\Delta x = \Delta z$	Grid size cells	Number of cells
0.05	78 × 54	4 212
0.03	130 × 90	11 700
0.02	195 × 135	26 325
0.01	390 × 270	105 300

RESULTS, 10% TANK FILLING RATE

Full grid convergence study has been performed for the lowest filling rate of 10%. Only selected graphs will be presented in this paper, but much more can be found in [14].

The first group of graphs presents ComFLOW results concerning fluid height at location WH03. Graphs in Fig. (10) show results for the single-phase flow and upwind differencing scheme **B2**. No significant improvement has been obtained with the **B3** scheme and the graphs are therefore omitted. The agreement with the experimental signal is quite satisfactory for all grid densities.

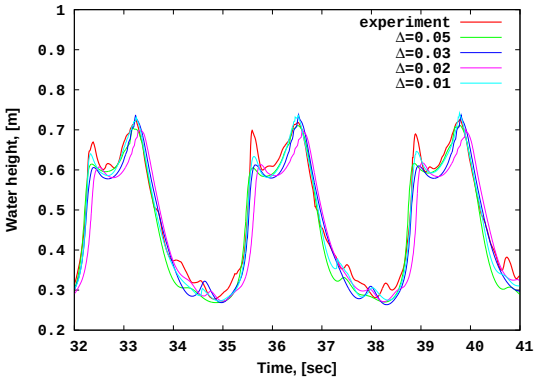

Figure 10. Fluid height at WH03, grid convergence, **B2**, 1-phase flow

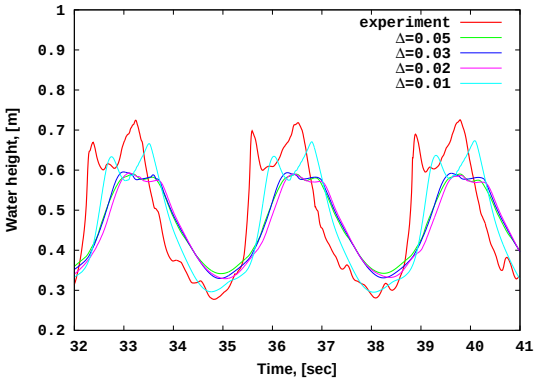

Figure 11. Fluid height at WH03, grid convergence, **B2**, 2-phase flow

Results obtained with the two-phase flow model are displayed in graphs Fig. (11) and Fig. (12). It can be seen that for the two-phase flow calculations it is necessary to use the 2^{nd} order upwind differencing scheme **B3**. Results obtained with **B2**, Fig. (11), are significantly over-damped, and only application of the finest grid, Δ=0.01, allows to approach the experimental result more closely.

Usage of the 2^{nd} order upwind differencing scheme **B3**, Fig. (12), improves results significantly. The results approach the experiment, although it can be seen that the two finest grids Δ=0.01, 0.02 produce somewhat unstable results. It must be underlined again that the two-phase flows with **B3** are very time consuming and that for Δ=0.01 the simulation has been cancelled at some stage due to an excessive CPU demands (the curve is marked with an asterisk in Fig. (12)).

Finally, results for all applied methods and for a "reasonably optimal" grid of Δ=0.03 are shown in Fig. (13). The term "reasonably optimal" is obviously subjective and is a compromise between maximum desirable accuracy and length of calculations.

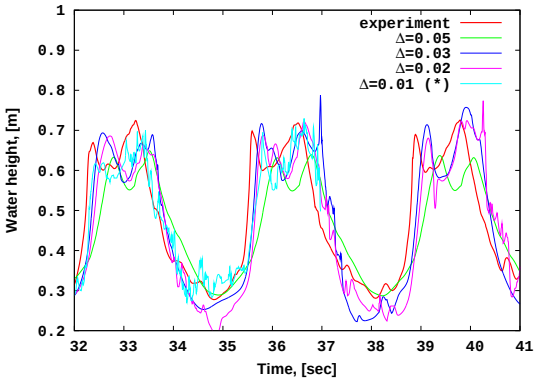

Figure 12. Fluid height at WH03, grid convergence, **B3**, 2-phase flow

A similar set of graphs is presented for fluid pressures at location P08, Fig. (14) through Fig. (17). The experimental pressure signal contains short peaks of very high values, and these peaks have been partially cut off the graphs in order to make the remaining curves more legible. It is not sure that these peaks recorded during experiments are the true result, and actually such experimentally obtained peaks deserve a separate discussion.

Numerically produced high value pressure peaks are also occassionally present and a possible explanation of their origin can be found in [4, 8].

Calculations employing the single-phase flow and upwind differencing scheme **B2** again produce quite satisfactory results for all tested grid densities, Fig. (14). And again, there was no significant improvement for the single-phase, **B3** algorithm.

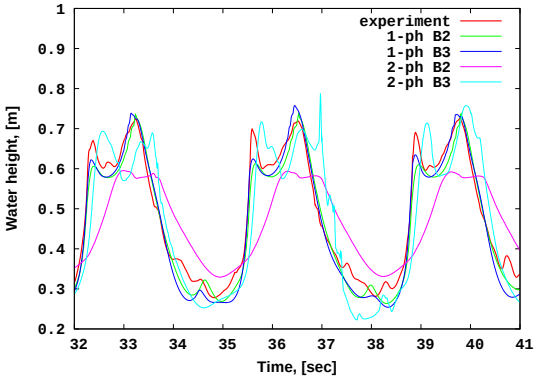

Figure 13. Fluid height at WH03, all methods for grid Δ=0.03

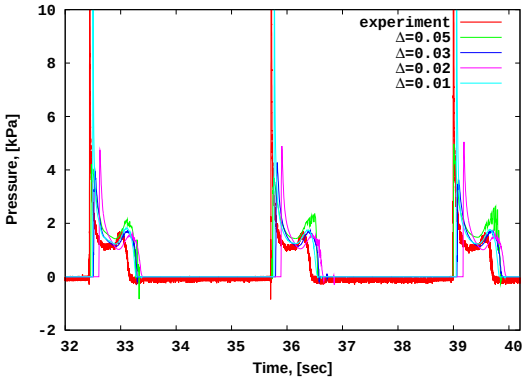

Figure 14. Pressure at P08, grid convergence, **B2**, 1-phase

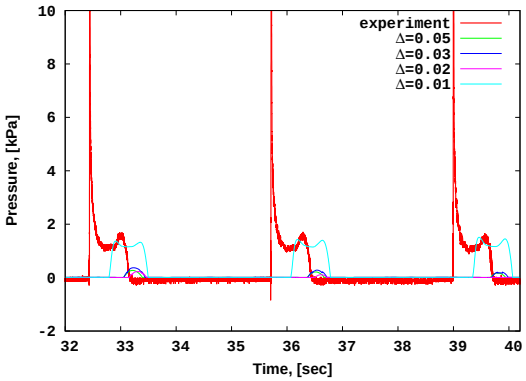

Figure 15. Pressure at P08, grid convergence, **B2**, 2-phase

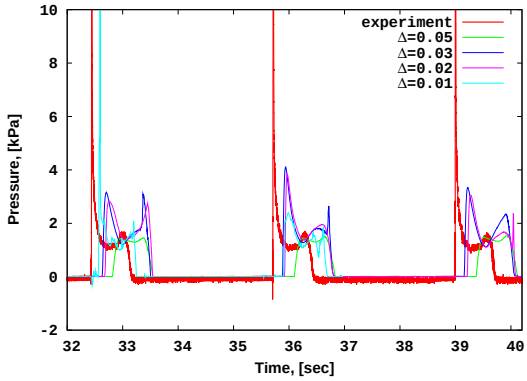

Figure 16. Pressure at P08, grid convergence, **B3**, 2-phase

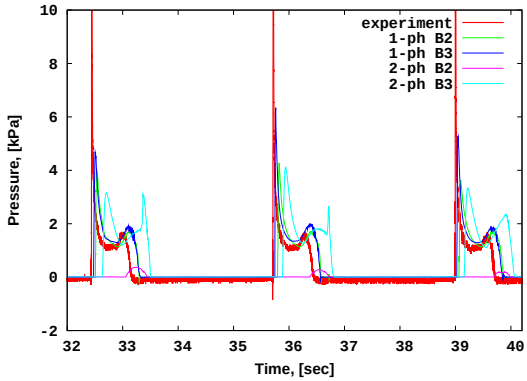

Figure 17. Pressure at P08, all methods for grid Δ=0.03

Application of two-phase fluid flow physics with **B2** upwind differencing scheme fails to produce a useful estimation of the pressure, Fig. (15). The fluid motion is over-damped and fluid does not even reach location of the pressure sensor P08, except for the finest grid case Δ=0.01 (and still no typical impact can be observed). The two-phase, **B3** solution fares much better, Fig. (16).

Results for all applied methods and grid of Δ=0.03 are shown in Fig. (17).

RESULTS, HIGHER TANK FILLING RATES

Results of the ComFLOW sloshing simulations for the higher tank filling rates of 25%, 70% and 95% are presented in graphs, Figs. (18-20), for the fluid height at WH03. Three other graphs, Figs. (21-23), show fluid pressures at the selected pressure sensor locations, listed in Tab. (2).

No grid convergence study is presented here, but rather results for the selected "reasonable" grid accuracy of Δ=0.03 and all four discussed methods. The results are commented in the Conclusions section. One remark is due, however. The fluid height graphs do not seem to be perfectly consistent, especially along flat parts of the curves, which can be seen particularly in Figs. (19-20). The fluid height probes used in experiments were electrical wires pasted to the tank's wall. The recorded values are actually lengths of the currently wet parts of a wire and by necessity are sensitive to air bubbles or a water-air foam which could be present along the wire span.

Such situation contaminates the recorded result. But it should also be noted that the fluid height reporting system in ComFLOW works in a very similar way. Authors are not aware whether a reliable cure for this problem exists.

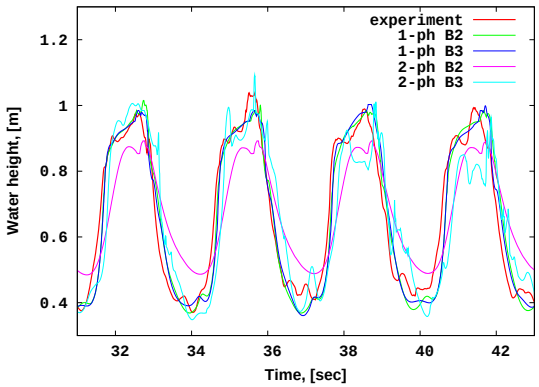

Figure 18. Fluid height at WH03, 25%, Δ=0.03

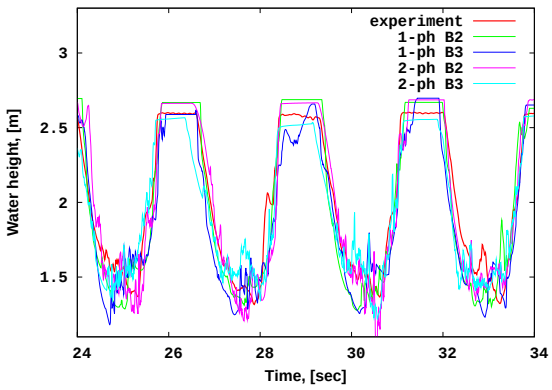

Figure 19. Fluid height at WH03, 70%, Δ=0.03

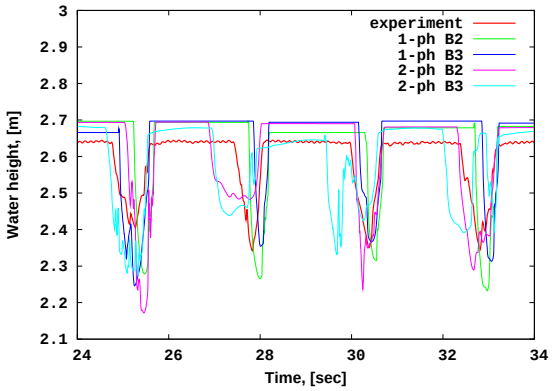

Figure 20. Fluid height at WH03, 95%, Δ=0.03

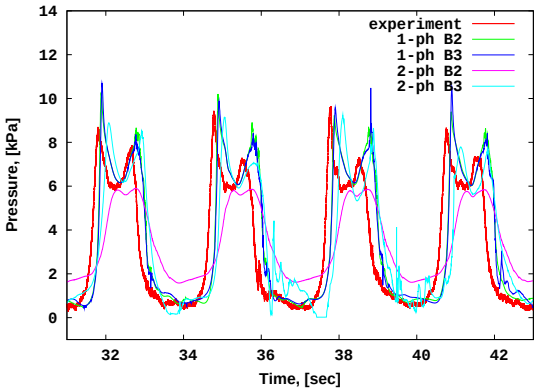

Figure 21. Fluid pressure at P04, 25%, Δ=0.03

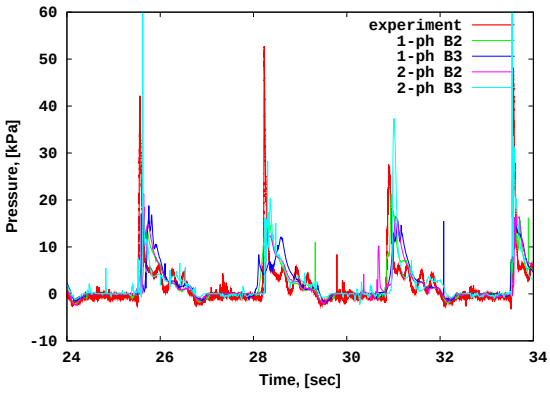

Figure 22. Fluid pressure at P02, 70%, Δ=0.03

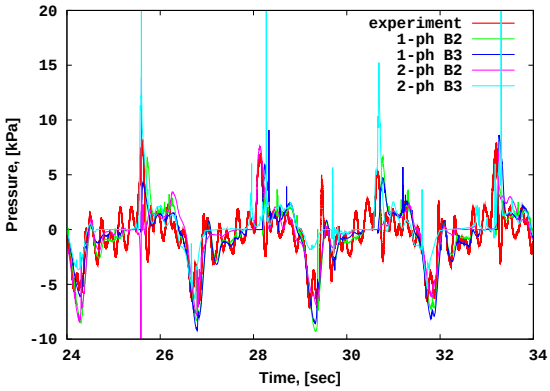

Figure 23. Fluid pressure at P08, 95%, Δ=0.03

CONCLUSIONS

1. It seems that for low filling rates of the tank, the single-phase physics and the 1^{st} order upwind differencing scheme **B2** give satisfactory results for both fluid height and pressure. No significant improvements have been obtained with usage of two-phase physics and **B3** upwind differencing scheme for low filling rates.
2. However, it is recommended to use the **B3** upwind differencing scheme if the two-phase fluid model is employed. The two-phase fluid flow motion is over-damped with **B2**.
3. For high filling rates of the tank, the fluid height and sloshing pressures are predicted reasonably well by all the presented methods. Currently it is not possible to recommend the best combination of physical model and upwind differencing scheme. It is believed that the two-phase and **B3** approach is the most applicable for high filling rates, but more studies are necessary in order to support this opinion.
4. A separate approach is necessary to deal with the experimentally produced pressure peaks. Such peaks appear in many experiments and can be related to a physical size of the used pressure sensor, local (structural) natural frequency of the experimental container, quality of the data acquisition equipment and other factors as well.
5. The problem of numerically produced pressure peaks should be also addressed. Typically, there are some theoretical and/or practical reasons related to the currently applied numerical algorithm itself. The numerically induced peaks, if their origin is known and explainable, can be removed by a reasonably designed peak-removal procedure. Such a procedure should be rather delicate and well-balanced, since it is quite easy to smooth-out the truly existing flow features. However, it is stressed that no filtering/smoothing procedure of any kind has been used in this paper.

It seems that the ComFLOW program is a viable alternative for the sloshing in a tank CFD simulation. Both fluid height and pressure can be predicted and the numerically obtained sloshing pressures are close the the experimental ones.

It is true that some of the reported simulations took many days to complete. Parallelization of the ComFLOW code is currently worked upon in order to alleviate the problem.

ACKNOWLEDGMENT

Authors would like to thank participants of the ComFLOW-2 Joint Industry Project for financial support and permission to publish the results.

REFERENCES

[1] Greco, M., Colicchio, G., and Faltinsen, O.M., 2005. "Application of a 2D BEM-Level Set Domain Decomposition to the Green-Water Problem". 20-th International Workshop on Water Waves and Floating Bodies, Longyearbyen, Norway.

[2] Peric, M., Zorn, T., El Moctar, O., Schellin, T.E, and Kim, Y-S., 2007. "Simulation of Sloshing in LNG-Tanks". In Proceedings, 26-th International OMAE Conference, San Diego, CA. Paper OMAE2007-29555.

[3] Yu, K., Chen, H-C., Kim, J.W., and Lee, Y-B., 2007. "Numerical Simulation of Two-Phase Sloshing Flow in LNG Tank Using Finite-Analytic Level-Set Method". In Proceedings, 26-th International OMAE Conference, San Diego, CA. Paper OMAE2007-29745.

[4] Wemmenhove, R., Luppes, R., Veldman, A.E.P., and Bunnik, T., 2008. "Application of a VOF Method to Model Compressible Two-Phase Flow in Sloshing Tanks". In Proceedings, 27-th International OMAE Conference, Estoril, Portugal. Paper OMAE2008-57254.

[5] Hirt, C.W., and Nichols, B.D., 1981. "Volume Of Fluid (VOF) Method for the Dynamics of Free Boundaries". *Journal of Computational Physics,* **39**, pp. 201–225.

[6] Kleefsman, K.M.T., 2005. "Water Impact Loading on Offshore Structures - A Numerical Study". PhD Thesis, University of Groningen, The Netherlands, November.

[7] Kleefsman, K.M.T., Fekken, G., Veldman, A.E.P., Buchner, B., and Iwanowski, B., 2005. "A Volume-Of-Fluid Based Simulation Method for Wave Impact Problems". *Journal of Computational Physics,* **206**, pp. 363–393.

[8] Wemmenhove, R., 2008. "Numerical Simulation of Two-Phase Flow in Offshore Environments". PhD Thesis, University of Groningen, The Netherlands, May.

[9] Bunnik, T., and Huijsmans, R., 2007. "Large Scale LNG Sloshing Model Tests". In Proceedings, 17-th International ISOPE Conference, Lisbon, Portugal.

[10] Bunnik, T.H.J., 2007. Large Scale Sloshing Model Tests. Technical Report 18378-1-PO, Maritime Research Institute Netherlands (MARIN), Wageningen, The Netherlands, August.

[11] Anderssen, R.S., and de Hoog, F.R., 1984. "Finite Difference Methods for the Numerical Differentiation of Non-Exact Data". *Computing,* **33**, pp. 259–267.

[12] Ralston, A., and Wilf, H.S., 1960. *Mathematical Methods for Digital Computers*. Wiley, New York.

[13] Lim, J.S., and Oppenheim, A.V. (Eds)., 1988. *Advanced Topics in Signal Processing*. Prentice-Hall, Englewood Cliffs, NJ.

[14] Iwanowski, B., 2008. ComFLOW-2 JIP: Benchmarks of the ComFLOW Program. Technical Report TR-2008-0049, FORCE Technology Norway AS, Sandvika, Norway, October.

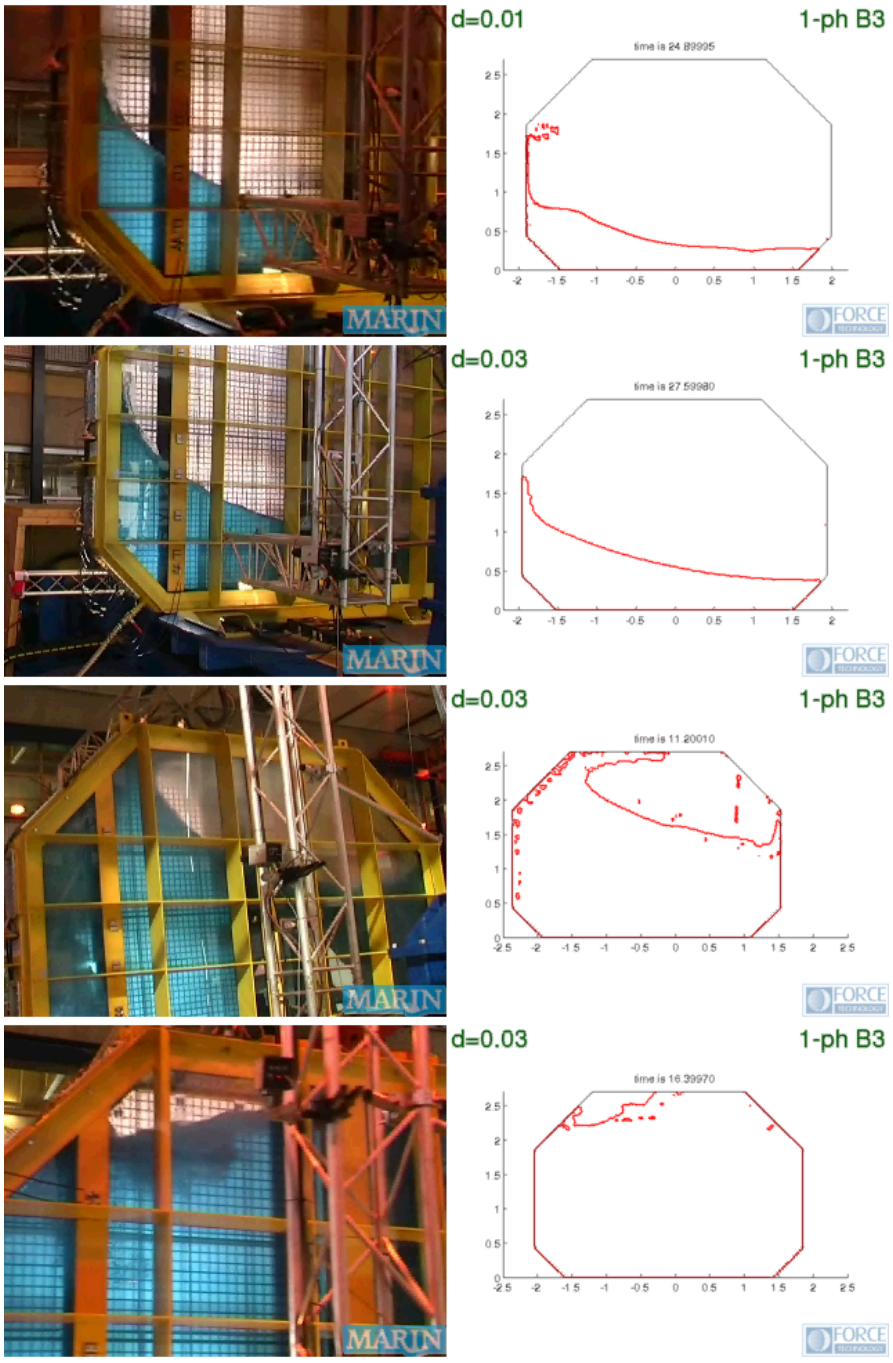

Figure 24. Synchronised video frames, from top: 10%, 25%, 70%, 95% filling rate

Appendix A: Synchronised Video Frames, Experiment and Calculations

The discussed sloshing experiments have been filmed with a digital camera. It is also possible to produce a video animation from each of ComFLOW calculations presented in the paper. The Appendix shows four synchronised frames composed from the experiment and the calculation, one frame for each of the discussed 10%, 25%, 70%, 95% tank filling rates.